Convection Battery—Modeling, Insight, and Review

Michael Gordon and Galen Suppes
Dept. of Chemical Engineering, University of Missouri, Columbia, MO 65211

DOI 10.1002/aic.14080
Published online March 18, 2013 in Wiley Online Library (wileyonlinelibrary.com)

Porous electrode theory was used to model performance of the convection battery using lithium iron-phosphate chemistry. The model results and underlying equations were able to quantify and extend previous interpretations of laboratory validation studies. These analyses substantiated the following conclusions on the performance of the convection battery: (a) flow in the convection battery can reduce concentration overpotentials by 99.9%, (b) both the ionic and electron conductivities of solid phases can have a major impact on convection battery performance, and (c) the solid-phase ionic conductivity of a porous separator is an important design parameter and is not considered by porous electrode theory as published to date. In view of the ability of the convection battery to overcome both bulk diffusion and liquid-phase effective conductivity limitations; the convection battery has an unprecedented potential to redefine the performance of large batteries. © 2013 American Institute of Chemical Engineers *AIChE J*, 59: 2833–2842, 2013
Keywords: diffusion (in membranes), electrochemistry, energy, membrane materials

Introduction

The convection battery uses a new cell configuration[1–5] with pumped-electrolyte convection to overcome bulk diffusion limitations. This article uses the porous electrode theory[6–10] model to interpret data, provides insight into the physiochemical properties that impact performance, identifies performance potential, and identifies the materials and configurations needed to attain the performance potential.

Table 1 summarizes potential advantages of batteries using convection cells. It is recognized that some of these advantages do not come without a price; however, that price becomes an increasingly small part of the total battery cost for large batteries. It is also important to recognize that these advantages could be applied to most battery chemistries—the exception is that the convection battery is not compatible with flow battery chemistries.

Both flow batteries and convection batteries use pumps to circulate electrolyte through electrodes as illustrated in Figure 1; however, beyond this similarity, they are substantially different. The convection battery pumps electrolyte directly from an electrode to its counter-electrode through a flow-permeable separator with the purpose of eliminating concentration overpotentials—the reagents are stored in solid phases as part of the electrodes. The flow battery[11–14] stores the reagents in one or both liquid electrolytes and uses flow to deliver the reagent to the electrode(s); the electrolyte of the anode is kept separate from the electrolyte of the cathode to avoid the mixing of reactive reagents. The combinations of reagents and electrolytes compatible with flow batteries vs. convection batteries are mutually exclusive.

Correspondence concerning this article should be addressed to G. Suppes at suppesg@missouri.edu.

Both convection and flow batteries have capital and operating costs associated with the pumping of electrolyte. Although the determination of pumping costs is an advanced aspect of development and design rather than research, at this research stage on convection batteries certain conclusions can be made about the relative pumping costs of convection vs. flow batteries.

As implicit from Figure 2, the capital costs associated with pumping in the convection cell are about half those of flow batteries.

The energy costs are primarily related to the volume that needs to be displaced—this is based on the assumption that pressure drop is less important for low-pressure-drop designs where the piping and connections tend to normalize pressure drops. Figure 2 illustrates the flow pattern for a flow battery and two options for the convection battery. The flow battery requires full displacement of the void volumes of the electrodes for full displacement of electrolyte, whereas the base case convection battery requires displacement of half of the electrode void volumes. This is because the goal of pumping in the convection battery is to displace one electrode volume into the counter-electrode rather than to introduce fresh electrolyte into both electrodes.

An option with the convection battery is to use baffles to direct electrolyte back-and-forth between electrodes several times before the electrolyte exits. Figure 2 illustrates how two baffles can reduce the volume of displacement relative to the flow battery from 2 to 0.67 L. A nine-baffle system would require 10% of the relative volume displacement. For the case where the pump is only needed 10% of the time, the convection battery would require about 1% of the energy of a comparable flow battery based on these assumptions.

The focus of this article is on modeling of convection battery performance and the conclusions that can be drawn from this modeling. Porous electrolyte theory provides one

Table 1. Design Options for the Convection Battery Architecture

Increased ion flux through separator/membrane	This would lower the cost for attaining increased current ratings in batteries. For larger batteries the goal is a >10× increase in limiting current (same battery configuration with and without flow). The goal is for a 50% decrease in the price for convection battery vs. diffusion battery at the same C rating
Control of ion flux	The goal is to be able to increase the current rating of a given convection battery by turning the pump on. For example, a PHEV battery that would only require that the pump be turned on during acceleration or rapid battery charging at a station
Heat removal	The goal is for the use of an in-line radiator that will remove heat at basically any needed rate
Safety	The goal is to reduce battery power by turning off the pump
Manufacturing/regeneration options	The goal is to be able to load or recharge an active material into an electrode of a battery from an exterior canister by flowing electrolyte through the electrode and controlling voltage to achieve desired electrodeposition (or other) loading
Li-plated anodes	The goal is to use a combination of flow, thicker separators, and charging cycles to allow the use of metallic (or plated) lithium in secondary batteries
Shelf life, fade, and parasitic reactions	The goal is to be able to routinely drain electrolyte from the battery as part of normal operation to extend shelf life, reduce fade, and reduce parasitic losses

of the most comprehensive approaches to modeling the phenomena occurring in the convection battery. Previous publications on the convection battery have described experimental systems, presented data, and provided qualitative interpretations of data. The purpose of this article is to quantify the previously only qualitative insight and to provide additional insight and interpretations of convection battery performance. All model solutions presented in this article are for the lithium iron-phosphate chemistry.[15,16]

Model Development

The model consists of both a one-dimensional (1-D) geometry and a two-dimensional (2-D) geometry. The 1-D geometry, with the length of the battery along the *x*-axis, is used to describe the liquid-phase material balance, the liquid-phase charge balance, and the solid-phase material balance and is split into four sections along the axis: the negative electrode (anode during discharge), the separator (sometimes referred to as the membrane), the positive electrode (cathode during discharge), and the circulating tube that directs the electrolyte through the pump and into the counter electrode. Positive flow is referred to as flow that is in the same direction as the Li^+ flow in the case of diffusion cell operation; more specifically, positive flow is where electrolyte exits the cathode, then enters the pump, and then enters the anode (counter electrode).

The 2-D geometry, with the length of the battery along the *x*-axis, corresponding to the 1-D model, and the particle radius along the *y*-axis, is used to describe the intercalation of lithium ions in the solid electrodes. This geometry is linked to the 1-D geometry at the upper boundary of the *y*-axis or the maximum particle radius. The values for the solid-phase concentration of lithium ions at this boundary are projected onto the corresponding *x*-axis value in the 1-D model and are used to calculate the exchange current between the solid electrodes and the electrolyte.

Porous electrode theory reduces to solving Eqs. 1–4 specific to this pseudo-1-D battery configuration where the anions and cations have single charges in a binary electrolyte: the liquid-phase material balance that provides concentrations of the cation and anion in the electrolyte

$$\epsilon \frac{\partial c_+}{\partial t} = D_2^{\text{eff}} \frac{\partial^2 c_+}{\partial x^2} - v^* \frac{\partial c_+}{\partial x} + \frac{\left(1-t_+^*\right)}{F} a i_n \tag{1}$$

the liquid-phase charge balance that provides a charge continuity via the liquid throughout the cell where

$$\kappa_2^{\text{eff}} \frac{\partial^2 \Phi_2}{\partial x^2} = \frac{2RT\kappa_2^{\text{eff}}}{F}\left(1-t_+^*\right)\frac{\partial^2 \ln c}{\partial x^2} - a i_n \tag{2}$$

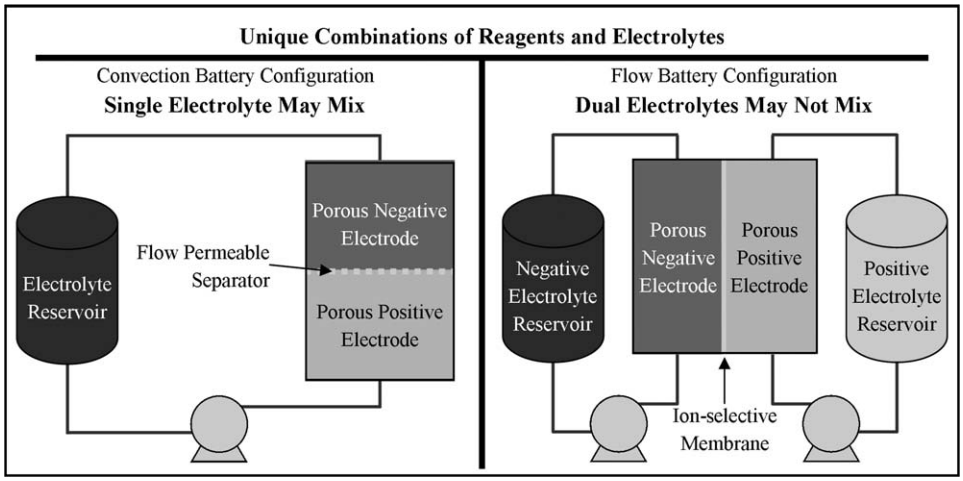

Figure 1. Illustration of convection vs. flow battery cells emphasizing the null overlap in combinations of reagents and electrolytes compatible with each type of cell.

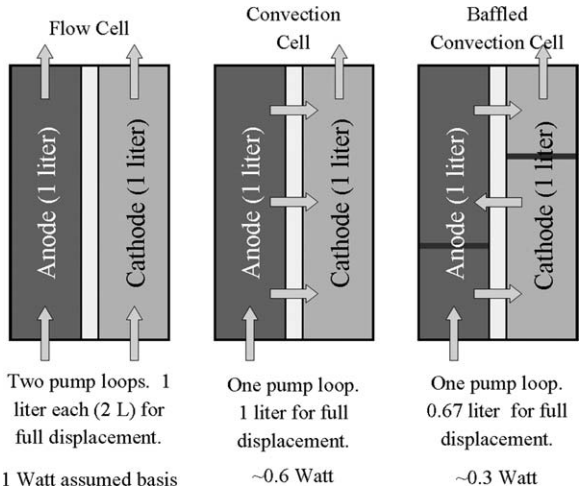

Figure 2. Comparison of flow patterns for standard flow battery design as compared to standard and baffled convection battery designs.

A basis is assumed of 1 L void volumes in electrodes and a 1 W basis for the flow battery.

the solid-phase material balance where

$$\frac{\partial c_s}{\partial t} = D_s\left[\frac{\partial^2 c_s}{\partial r^2} + \frac{2}{r}\frac{\partial c_s}{\partial r}\right] \tag{3}$$

and the solid-phase charge balance where

$$-\kappa_1^{\text{eff}}\frac{\partial^2 \Phi_1}{\partial x^2} = -a i_n \tag{4}$$

The Butler–Volmer equation (Eq. 5) is used to relate the overpotential driving force for the transfer of mass to/from the solid electrode and the electrolyte

$$i_n = i_0\left[\exp\left(\frac{\alpha_a F \eta_s}{RT}\right) - \exp\left(-\frac{\alpha_c F \eta_s}{RT}\right)\right] \tag{5}$$

Equations 6 and 7 express the Butler–Volmer terms in terms of parameters related to the materials of the battery

$$\eta_{s1} = \Phi_1 - \Phi_2 - U_1 \tag{6}$$

$$i_0 = F(k_a)^{\alpha_c}(k_c)^{\alpha_a}\left(c_{s,\max} - c_s\right)^{\alpha_c}(c_s)^{\alpha_a} \tag{7}$$

Additional equations that can be used to provide insight into the performance are the ion flux equations for the anion (Eq. 8) and the cation (Eq. 9)

$$\boldsymbol{N}_- = -D_2^{\text{eff}}\frac{dc_-}{dx} - \frac{\boldsymbol{i}_2 t_-^*}{F} + c_-\boldsymbol{v}^* \tag{8}$$

$$\boldsymbol{N}_+ = -D_2^{\text{eff}}\frac{dc_+}{dx} + \frac{\boldsymbol{i}_2 t_+^*}{F} + c_+\boldsymbol{v}^* \tag{9}$$

Figure 3 presents a case of the limiting performance of the solution to Eqs. 1–7 for the limiting case of the diffusion cell with a velocity of zero. In the limit of no flow, the model generates typical concentration profiles for a diffusion cell. With increasing velocities, the concentration profiles flatten. This type of limiting behavior is consistent with

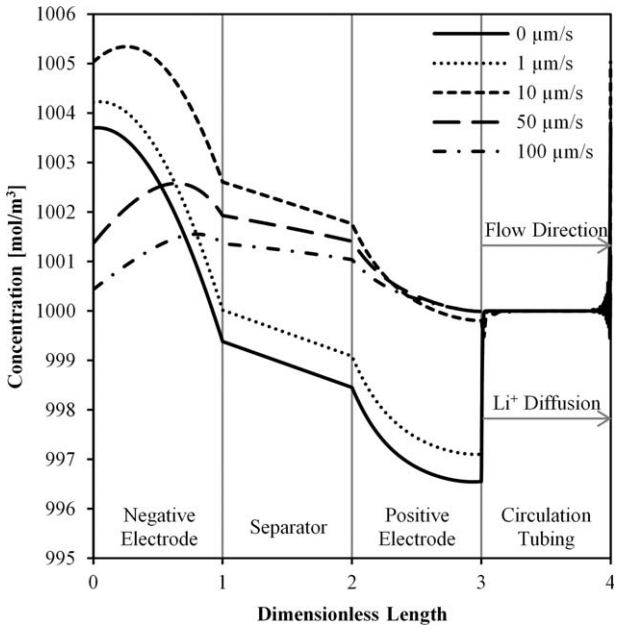

Figure 3. Concentration profiles for porous electrode theory model using a combination of parameter values from literature and high diffusivity.

expectations and serves to validate that the model does not violate known trends in behavior.

At low velocities the circulation tube shows transient behavior, with the concentration in the middle of the tube not impacted by the flow for the time frame of this simulation. The formation of maxima concentration in the anode is a result of a combination of dilution due to electrolyte flow from the circulating tube and diffusion.

The flat profile of the circulation tube is a result of the volume of electrolyte in the circulation tube being relatively large and the cross-sectional area (for mass transfer) being relatively low.

Model Solutions

Model parameters (diffusivity and solid-phase Li^+ diffusivities) were fit to data for the lithium iron-phosphate cell that were previously published.[5] Figure 4 shows the model lines superimposed over the experimental data. The model fit qualitatively agrees with experimental data. For both the model and the experiment, the performance with flow is considerably better than performance without flow. For initial studies, the convection cell was able to provide currents up to five times greater than the diffusion cell while realizing similar utilization of active materials. Once the parameters were fitted to the model, the performance of the cell was simulated for both positive and negative flow conditions. Figure 5 summarizes the voltage drops across the separator vs. time as generated by the simulation at a discharge current density of 2.65 mA/cm^2.

As Li^+ is the reactive ion that must move from the anode to the cathode during discharge, it is reasonable to hypothesize that the electrolyte should flow from the anode to the cathode during discharge for the best results; this flow direction is referred to as a positive flow direction. These diagrams show voltage drop (overpotential) across the separator

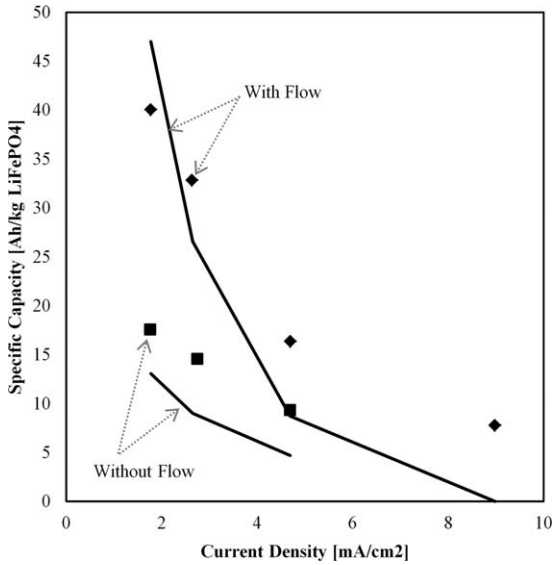

Figure 4. Performance curves for the convection vs. diffusion battery cell using same loadings and test cell.

Flow was turned off on the convection cell to obtain diffusion cell performance. The symbols are for experimental constant resistance discharge with capacity being measured to a cut-off voltage of 2.0 V from a previous publication.[5] The lines are model fits using a constant current discharge.

for positive vs. negative flow as a function of time at the same constant current.

The following are observed: (a) for the case of the diffusion cell (velocity = 0), the overpotential increases as the concentration gradients increase in the separator, (b) flow substantially reduces the voltage drop (overpotential) relative to the diffusion cell, (c) higher velocities result is an essentially constant voltage drop due to the elimination of concentration gradients in the convection-dominated cell, and (d) the flow direction impacts the transitional behavior between diffusion-dominated mass transport at low velocities and convection-dominated mass transport at high velocities. The hypothesis is valid in the transition from diffusion-dominated to convection-dominated behavior but does not apply at high flow rates (high velocity).

From Figure 5, the initial overpotential across the separator is 0.0489 V for all of the flow rates. Initially, the cell is in equilibrium, so there are no concentration gradients, and, thus, no concentration overpotentials. Therefore, this 0.0489 V is the ohmic overpotential in the separator, which is constant because the model uses a constant current discharge. The total overpotential at 2100 s into the discharge with no flow is 0.100 V, which translates to a concentration overpotential of 0.051 V by subtraction of the ohmic overpotential. At 2100 s, for velocities of both +118 and −118 μm/s, the concentration overpotential is only 2×10^{-5} V. This is a 99.9% reduction in the concentration overpotential in the separator with flow in either the positive or the negative direction.

At low velocities such as +0.1 and −0.1 μm/s, the flow direction can have a significant impact on the concentration overpotential as predicted. At 2100 s into discharge, the concentration overpotential for +0.1 μm/s is 0.027 V, and it is 0.059 V for a velocity of −0.1 μm/s. However, as the velocity increases, the effect of flow direction is diminished as seen at 118 μm/s.

Two convection cells were cycled with a 2.19 mA/cm^2 constant current charge and a 2.65 mA/cm^2 constant current discharge cycles—one with a velocity of +118 μm/s and the other with a velocity of −118 μm/s. The assembly of these convection cells has been reported previously.[5] The cells with a positive flow had a capacity of 12 A h/kg of $LiFePO_4$, and the cells with a negative flow rate had a capacity of 13 A h/kg of $LiFePO_4$. The <10% difference between these two cells is within the experimental error and indicates that the direction of flow has little effect at high flow rates. In the model, when flow does make a difference, positive velocities would result in a larger capacity, which is contrary to the minor difference in performance that was detected.

Figure 6 summarizes the concentration profiles as modeled for different velocities at 2100 s into the discharge based on parameters fitted to cell voltage data with a discharge current density of 2.65 mA/cm^2. For positive flow profiles, the

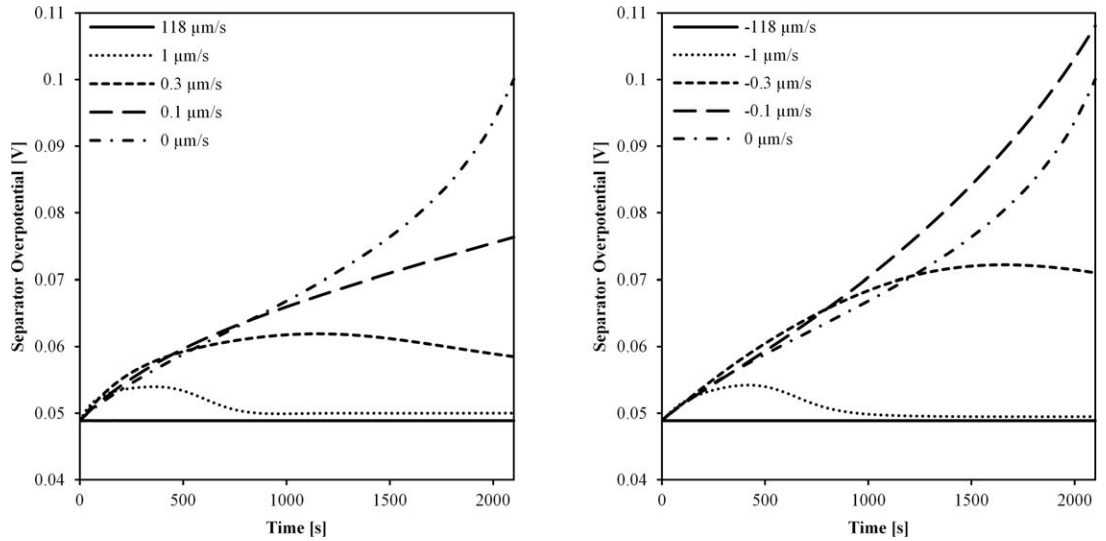

Figure 5. Overpotential in the separator as a function of time for different velocities, with positive flow in the left graph and negative flow in the right graph.

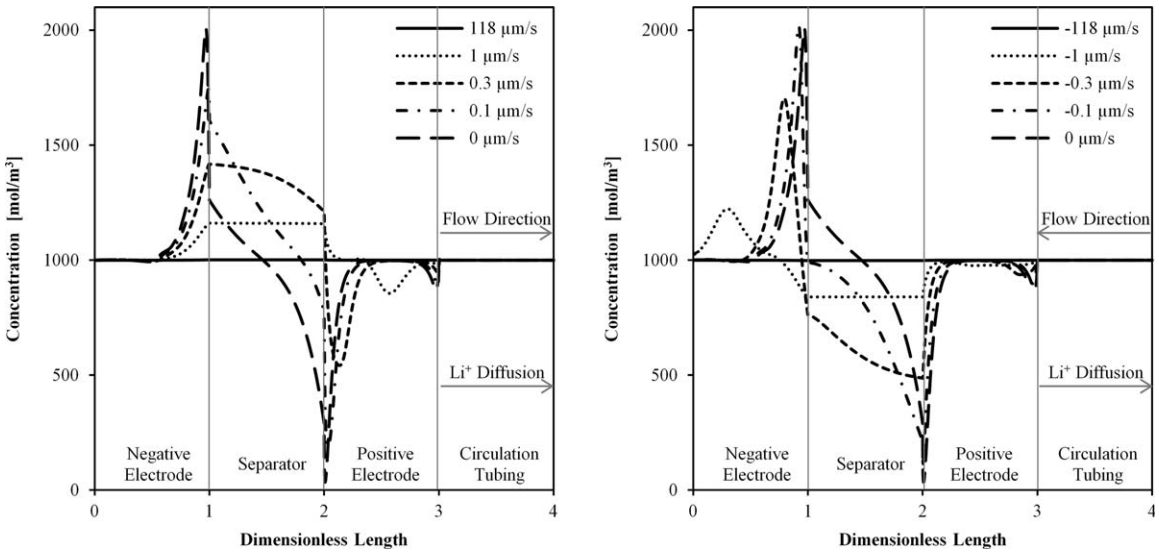

Figure 6. Simulated concentration profiles (concentration of Li^+ that is equal to anion concentration for binary electrolyte) for positive and negative flow.

concentration in the separator transitions from: (a) a gradient that dominated the driving force for Li^+ mass transfer, (b) to a fairly flat Li^+ concentration profile at moderate flow rates where ion concentrations are higher in the separator than in the convection tube, and (c) to a substantially flat concentration profile at higher flow rates.

For negative flow, the convective flow substantially pushes the Li^+ generated in the anode back into the anode, forming an accumulation in the anode next to the separator. At moderate flow rates, the flow of lithium ions in the separator is less than the average bulk concentration. which is opposite in trend relative to the positive flow direction. This indicates that Li^+ is undergoing a net pumping from the anode to the cathode through the circulating tube rather than through the separator.

For flow in the positive direction, increased concentrations of Li^+ in the separator translate to a pumping of the active Li^+ cation from the anode to the cathode through the separator. For negative flow rates, the net pumping of Li^+ occurs through the circulating tube.

With no flow the maximum deviation in concentration from the equilibrium concentration of 1000 mol/m^3 is 1021 mol/m^3, whereas with a velocity of +118 μm/s the maximum deviation is 1.52 mol/m^3. This is the same maximum deviation for a velocity of −118 μm/s.

The delivered cell voltages of Figure 7 reflect overpotential trends in the separator. At 2100 s into the discharge the cell voltage is 0.283 V higher with a high flow rate than with no flow regardless of flow direction. The difference in voltage losses (overpotentials) between cells, with flow and without flow, is attributed to the concentration overpotential losses, as quantified in the separator, being extended over the entire battery cell. It should be noted that laboratory experiments were performed at velocities of 118 μm/s, and at those conditions the direction of flow had no impact on the cell voltage, which is consistent with the simulations summarized in Figure 7.

Diffusion Limit of Performance

Application of the flux equations (Eqs. 8 and 9) across a control volume around the cathode (see Figure 8) can be used to quantify the observed phenomena. The flux equations are applied at locations along the axial distance (× dimension). Equations 10 and 11 are charge balances applied over the cell with positive terms for entering conditions (left) and negative terms for exiting conditions (right) when there is positive flow. The salt concentration c is used in the following equations, which is equal to both the anion and the cation concentrations because of electroneutrality

$$\text{Current Flux (constant)} = \Delta \boldsymbol{N}_- = -D_2^{\text{eff}} \Delta \frac{dc}{dx} - \frac{t_-^*}{F} \Delta \boldsymbol{i}_2 + \boldsymbol{v}^* \Delta c \tag{10}$$

$$\text{Current Flux (constant)} = \Delta \boldsymbol{N}_+ = -D_2^{\text{eff}} \Delta \frac{dc}{dx} + \frac{t_+^*}{F} \Delta \boldsymbol{i}_2 + \boldsymbol{v}^* \Delta c \tag{11}$$

A pseudo-steady-state (PSS) is assumed as a limiting behavior similar to the diffusion and high flow limits. The PSS condition is the condition defined as the concentration gradient is fully developed across the separator and does not vary much with short increments of time. The PSS condition is approximated by a battery where the solid-phase stored reagents in the electrodes are only partially depleted at all locations and have an activity that is independent of the degree of depletion at the microscopic level in the materials of the electrodes.

When relating the PSS performance to actual cell performance, the primary adjustments to the PSS system are: (a) accumulation of ions in the anode and cathode and (b) variation in the activity of reagents in the solid phases of the electrodes. Both of these "real battery" variations substantially do not detract from the conclusions made by the PSS analysis, because they do not vary the physiochemical properties of the electrolyte and the conclusions made by the following PSS analysis are in terms of the physiochemical properties.

Evaluating the anion flux equation (Eq. 10) for PSS diffusion (flow at 0 m/s) at the left surface of the control volume, the following are observed: (a) there is no net flux of anions and (b) the velocity is zero. Therefore, the anion flux equation reduces to two terms: (a) the concentration-based

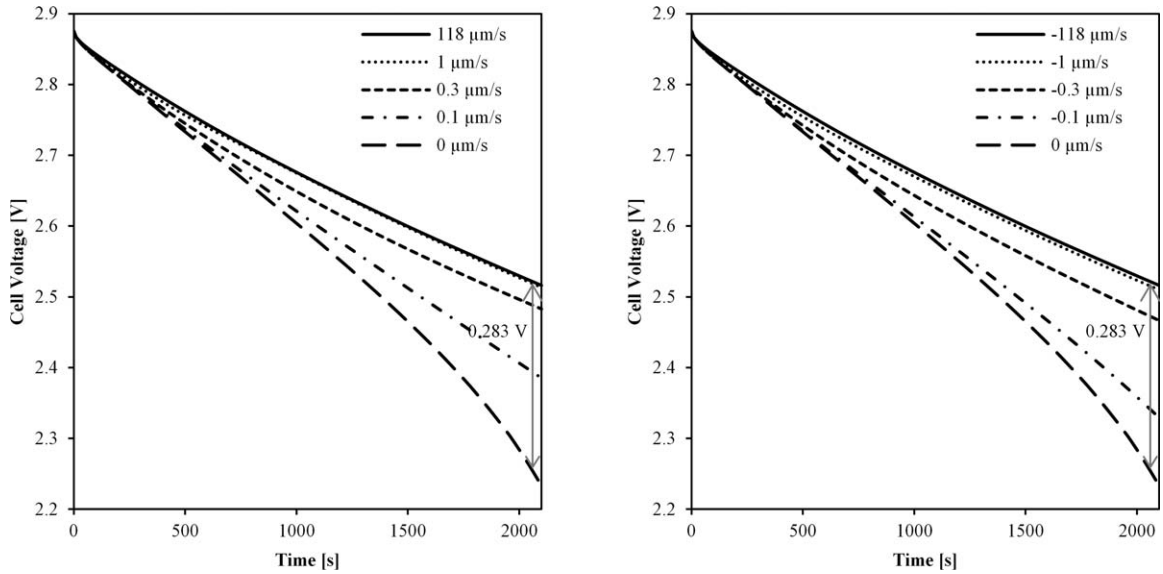

Figure 7. Cell voltages as provided by simulation for various positive and negative velocities to emphasize the effect on total overpotential in the cell.

diffusion driving force for flow to the cathode and (b) the balancing migration term of anions being attracted to the positive lithium generation (minor surplus) on the anode. Taking this into account and the fact that $\boldsymbol{i}_2$ is zero at the right surface of the control volume, the following equation can be obtained

$$\boldsymbol{i}_2 = -\frac{F}{t_-^*} D_2^{\text{eff}} \frac{dc}{dx} \tag{12}$$

The cation flux equation (Eq. 9) shows the cation flux is driven by complementary diffusion and migration terms. Both diffusion and migration are determined by the physiochemical properties of the fluid electrolyte (and possibly the solid).

Equation 12 diffusion limit of $\boldsymbol{i}_2$ can be substituted into Eq. 9 to provide Eq. 13. Equation 13 indicates that the performance of the diffusion cell (other than accumulation terms) is dominated by the physiochemical parameters: liquid-phase diffusivity and the transference number

$$\text{Constant Current} = \boldsymbol{N}_+ = -\frac{D_2^{\text{eff}}}{t_-^*} \frac{dc}{dx} \tag{13}$$

High Flow Limit of Performance

At high flow rates, flat concentration profiles are in both the separator and the circulation tube. The anion flux equation (Eq. 10) simplifies by setting the concentration gradient equal to zero. At high flow rate, this balance equation results in a form where bulk diffusivity drops out of the equation and does not impact performance.

For PSS analysis of the control volume, there is no accumulation (or consumption) of anions in the cathode, and so, $\Delta \boldsymbol{N}_-$ of Eq. 10 goes to zero to yield Eq. 14. The interpretation of this equation is that the amount of Li^+ that reacts at the cathode is equal to the amount of anions that migrate from the system in response to electrical potentials

$$0 = -\frac{t_-^*}{F} \Delta \boldsymbol{i}_2 + \boldsymbol{v}^* \Delta c \tag{14}$$

The same observation of near-zero concentration gradients for convective flow can be applied to Eq. 11 resulting in Eq. 15, where a constant current of operation is equal to a term containing the concentration difference and migration currents. A prominent mechanism of cation mass transfer is from flow of the electrolyte where the salt (anion and cation pairs) concentration is different for entering and exiting streams

$$\text{Constant Current} = \Delta \boldsymbol{N}_+ = \frac{t_+^*}{F} \Delta \boldsymbol{i}_2 + \boldsymbol{v}^* \Delta c \tag{15}$$

Additional, important observations include: (a) bulk diffusivity has minimal impact on performance at high flow rates and (b) voltage changes (overpotentials) that occur in the electrolyte must originate from the migration term in the form of ohmic losses.

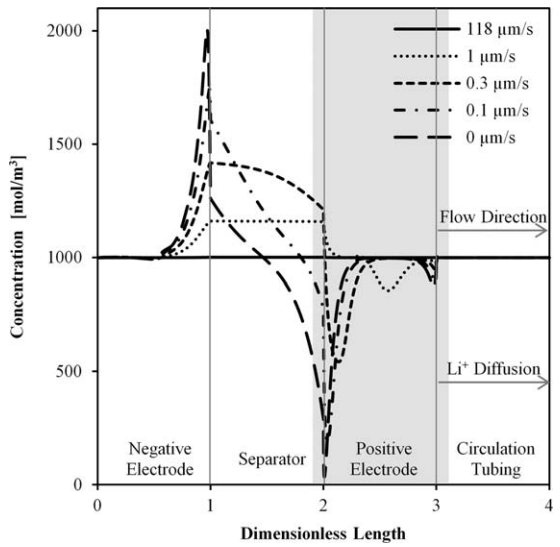

Figure 8. Illustration of control volume (shaded area) used to interpret performance.

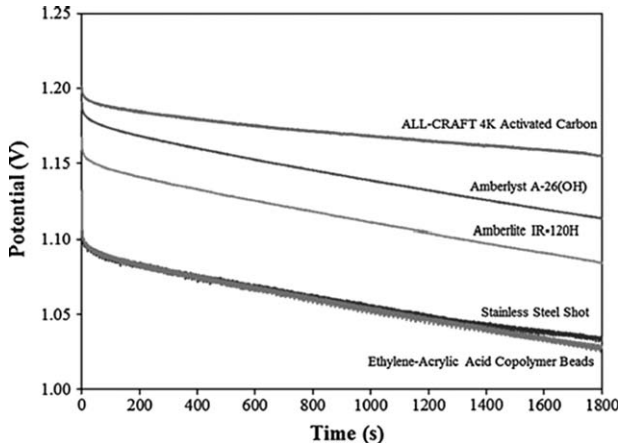

Figure 9. Impact of different packing media in the separator on performance of zinc-alkaline convection cells.[2]

In a binary electrolyte, the current $\boldsymbol{i}_2$ is calculated by Eq. 16, which relates $\boldsymbol{i}_2$ to the overpotentials

$$\boldsymbol{i}_2 = -\kappa_2^{\text{eff}} \nabla \Phi_2 + \frac{2RT\kappa_2^{\text{eff}}}{F}\left(1-t_+^*\right)\left(1+\frac{d\ln f_\pm}{d\ln c}\right)\frac{1}{c}\frac{dc}{dx} \quad (16)$$

Recognizing the flat concentration profiles at high flow rates at the entering and exiting conditions, the concentration term goes to zero, and by applying this equation to the control volume, Eq. 16 can be used to solve for $\Delta \boldsymbol{i}_2$ and be used to eliminate this term from Eq. 15 to arrive at Eq. 17

$$\Delta \boldsymbol{N}_+ = -\frac{\kappa_2^{\text{eff}} t_+^*}{F}\Delta\frac{d\Phi_2}{dx} + \boldsymbol{v}^*\Delta c \quad (17)$$

Hence, at constant current and PSS, the physiochemical properties that have an impact on overpotentials are the transference numbers and effective conductivity. Convective flow substantially eliminates bulk liquid diffusivity as a source of overpotential. Hence, overpotential arises from two primary sources in the liquid: (a) boundary-layer diffusion between electrode solid phases and the flowing electrolyte and (b) migration overpotentials as originating from transference numbers and effective ion conductivity.

Impact of Solid Matrices on Ion Conductivity

Figure 9 summarizes previously reported voltage profiles for a zinc-alkaline convection battery at a constant high flow rate (out of transition region) and resistance load.[2] The data illustrate how different solid phases in the separator can result in different overpotential losses associated with these changes in the test cell. The differences between voltages (differences are over potential differences) between the media are relatively constant.

In view of the previous conclusion that the overpotential of the separator at high flow rates is primarily a function of the ion-ohmic losses (specifically, the product $\kappa_2^{\text{eff}} t_+^*$) in the separator, the variations of performances illustrated in Figure 9 indicate that transference numbers and effective ion conductivities are functions of the solid material properties in the separator. This implies a surface, boundary layer, and/or solid state transport mechanism for ions in the separator. Figure 10 illustrates a separator with ion convection through the pore and cation migration through the membrane ion exchange polymer.

Solid-phase-related ion transport mechanisms are most important in liquid chromatography resins (as used for some of the experiments summarized in Figure 9). Ion exchange membranes are known to have ion transport properties,[17,18] and advancement of these membranes is an active area of research.[19–21]

Parallel bulk convection and resin-phase migration transport mechanisms are essential to understanding convection battery performance. At present, porous electrode theory uses one effective conductivity κ_2^{eff} to characterize the electrical properties of the separator and electrodes—an adjustment in this theory is needed to simulate the parallel mechanisms of Figure 10. For the convection battery, ions may migrate both through the liquid in pores and through/on the solid that forms the pores.

This conclusion must extend to the electrode properties. Furthermore, in the convection cell, it is the ion counter to the reacting anion of the electrolyte phase that relies on the solid matrix for transport. The reacting ion relies on convective flow for transport.

The activated carbon of Figure 9 is an ultra-high surface area carbon,[22] the Amberlyte and Amberlyst are liquid chromatography resin beads, and the steel and copolymer are presented as substantially inert solids. Both solid-phase surface area and ionic site density benefit the ability of solid materials in the separator to reduce ion-ohmic overpotentials. The Figure 4 data are consistent with a solid-phase ion transport mechanism that is robust at higher amperages, and the

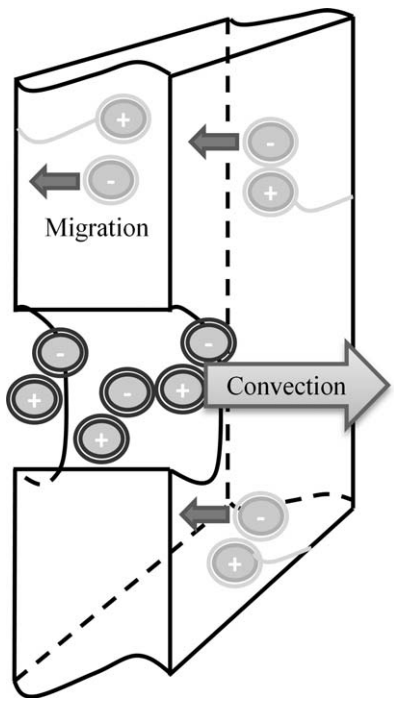

Figure 10. Illustration of transport in the separator of a convection battery where convection occurs through pores and anion migration is dominated by a path through the ion membrane material phase.

Migration through the polymer phase of the separator is believed to be the most effective migration mechanism.

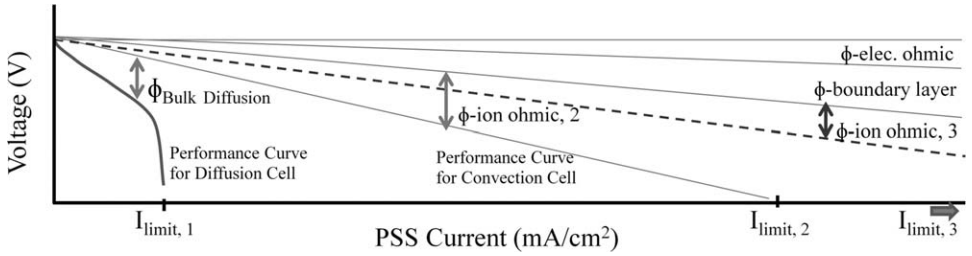

Figure 11. Illustrative PSS performance curves.

The lowest of the lines represents a diffusion cell performance curve and limiting current with the breakdown of overpotentials as indicted. The lowest straight line is the performance curve for a convection battery that has no bulk diffusion limitation. The dashed like is the performance curve for the convection battery with materials optimized for increased anion diffusivity.

poor fit of the model could be attributed to the lack of the ability of the model to include supplementary solid-phase ion mass transfer. Higher κ_2^{eff} diminish the impact of i_n on voltage drop in the electrolyte.

Implications on Convection Battery Performance

Qualitative PSS battery performance curves that break out example overpotentials are summarized in Figure 11. Bulk diffusion in the electrode and separator will typically increase significantly when the limits of a cell are pushed, eventually producing large overpotentials and a limit to current in that cell ($I_{\text{limit},1}$). The figure illustrates the overall performance curve for the diffusion cell (lowest curve on figure) where bulk diffusion overpotentials ultimately and largely determines the limiting current.

Bulk diffusion limitations are substantially eliminated in the convective battery. The new performance curve for the convective cell tends to be more linear and have a much greater limiting current ($I_{\text{limit},2}$). The ohmic losses tend to be linear with current and liquid-phase ion-ohmic overpotentials would tend to dominate the overpotential losses for well-engineering solid materials. The illustrated approximate 5× increase in limiting current was observed in recent studies in the convection cell.[5]

As illustrated in Figure 9, the solid matrix of separator materials and electrodes can have a significant impact on the ohmic losses. With improved materials that reduce ion-ohmic overpotentials, further increases in limiting currents can be realized. These could readily be 10× times the limiting current of the diffusion cell as illustrated by the dashed line; the limiting currents may be considerably more than 10× that of the diffusion cell.

An extrapolation of Figure 11 illustrates a significant performance advantage of the convection battery where power output (or input for charging) can be plotted against limiting current by multiplying the x-axis current times the y-axis voltage. More to the point, elimination of diffusion results in higher limiting currents and much higher maximum power output (or power input during charging). During charging, the input power would be from the charging source and significant reductions in charge times would be possible.

Significant reductions in charge times, reduced separator costs (thicker electrodes), and use of electrolyte flow to control power output are all advantages with potentially significant implications. On the topic of safety, thicker electrodes translate to a reduced potential for runaway reactions. And, the optional ability to drain electrolyte from the battery can be used as an ultimate safety control to shut down the battery if a runaway reaction is detected.

Parallelism of Electrode Overpotentials

Four sources of overpotential in a battery electrode include: (a) ohmic losses for electron transport in the solid, (b) ohmic losses for ion transport in the liquid, (c) a boundary layer (including nanopore diffusion) associated with reaction and transport from the solid surface to the bulk liquid, and (d) (proposed) ohmic losses for ion transport in/on the solid. Standard porous electrode theory does not account for the solid-phase ion transport; however, Eq. 6 relates the boundary-layer overpotential to the solid and liquid voltages.

Figure 12 further illustrates how the potential difference between points in the solution (point at Φ_A) and at the current collector (Φ_B) can be calculated via different paths. This indicates that these four sources of overpotentials act in parallel (as well as series) to produce an overall overpotential.

More specifically, the upper path for calculating $\Phi_A - \Phi_B$ as illustrated in Figure 12 proceeds substantially through the solid phase, whereas the lower path proceeds substantially through the liquid. The implication is that the use of a highly conductive solid phase (or solid with ion conductivity) can be used to minimize the adverse impacts of a low liquid effective conductivity.

The convection battery substantially eliminates bulk diffusion overpotentials, and so, the implication of being able to reduce the impact of remaining liquid overpotentials substantially increases the upper limits of what is possible with the convection battery.

Another way of considering this parallelism is recognizing that the term ai_n can be eliminated between the solid and electrolyte ion balance terms (Eqs. 2 and 4) resulting in an equation where the voltage drop in the electrolyte is related to the voltage drop in the solid. The magnitude of this interdependence is proportional to $\kappa_2^{\text{eff}}/\kappa_1^{\text{eff}}$.

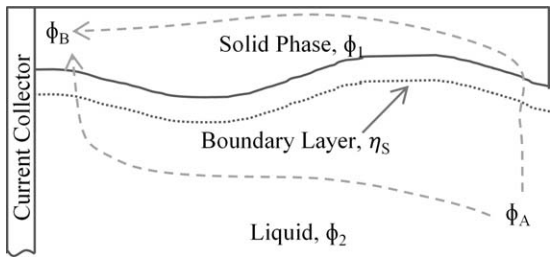

Figure 12. Illustration of different paths from the pore of an electrode to the current collector for realization of the potential difference $\Phi_A - \Phi_B$.

Conclusions

The following conclusions result from the modeling work and associated analysis of the balance equations:

- The convective battery is able to use fluid flow to reduce bulk diffusion overpotentials by 99.9%.
- As a result, bulk diffusivity has a substantially diminished impact on cell performance.
- The primary mechanism of reactive ion transport to and from electrodes in a convection cell is the $[\boldsymbol{v}^*\Delta c]$ term.
- Counter-ion (counter to reactive ion) transport emerges as a prominent overpotential that leads to a limiting current in the convective battery.
- This counter-ion-ohmic overpotential is highly dependent on the quantity $\kappa_2^{\text{eff}} t_+^*$.
- The solid matrix of separators (and electrodes) can have a significant impact on counter-ion-ohmic overpotential. Both the density of ion sites and surface area impact the ability of the solid matrix to reduce overpotentials.
- The electrolyte flow direction has an impact on the performance of the convection battery, but the impact is only moderate and only at the transition from diffusion-dominated to convection-dominated performance.
- In view of the parallelism of overpotential losses in electrodes, the limitations of low effective conductivities of the liquid phase can be substantially overcome by increasing the electronic (and possibly, the ionic) conductivities of the solid phase of the electrode.

As with the evolution of many chemical processing unit operations, there is a point where engineering design has an ever-increasing impact on scaling up and performance, the convection battery relies on an increasing amount of engineering science, as opposed to basic science, to achieve ever-increasing levels of performance. The convection cell demonstrated a 5× increase in the current density at the same capacity utilization as a diffusion cell.[5] Separator materials can limit the performance; improved separator materials have the potential for >>10× increases in limiting currents.

Acknowledgments

This work was funded by National Science Foundation grant number 1233250. Support for earlier experimental studies was provided by the California Energy Commission. Their supports are greatly appreciated.

Notation

ϵ = volume fraction
c, c_-, c_+ = concentration of salt, anion, and cation in electrolyte, respectively
c_s = solid-phase concentration of reagent
$c_{s,max}$ = max. solid-phase concentration
D_2^{eff} = effective salt diffusivity in electrolyte ($\epsilon^{1.5}D_2$)
D_s = diffusivity of lithium in the solid particles
r = particle radius
F = Faraday's constant, 96,485 C/mol
$\boldsymbol{v}^*$ = molar average velocity
$\kappa_2^{\text{eff}}, \kappa_1^{\text{eff}}$ = effective conductivity of the liquid ($\epsilon^{1.5}\kappa_2$) and solid (1 subscript), respectively
a = interfacial area of electrode solid divided by the volume of the electrode
i_n = charge being transferred to/from solid from/to electrolyte in electrode in current per interfacial area
i_0 = exchange current density
$\boldsymbol{i}_2$ = net current transported by liquid per cross-sectional area (perpendicular to axial dimension) of electrode
Φ_2, Φ_1 = potential of the liquid (1) and solid (2) phases, respectively
η_s = surface overpotential
U_1 = equilibrium voltage of the electrode
R = ideal gas constant
T = absolute temperature
t = time
$\boldsymbol{N}_-, \boldsymbol{N}_+$ = flux of anions (−) and cations (+), respectively
t_+^*, t_-^* = transference number of the cation (+) and anion (−), respectively, with respect to the solvent
α_a, α_c = apparent transfer coefficient for the anodic and cathodic reactions, respectively
k_a, k_c = reaction rate coefficient for the anodic and cathodic reactions, respectively, on the positive electrode
$f_\pm$ = the mean molar activity coefficient
x = distance along the length of the cell

Literature Cited

1. Suppes GJ, Sawyer BD, Gordon MJ. High-energy density flow battery validation. *AIChE J*. 2011;57(7):1961–1967.
2. Sawyer B, Suppes G, Gordon M, Heidlage M. Impact of electrode separator on performance of a zinc/alkaline/manganese dioxide packed-bed electrode flow battery. *J Appl Electrochem*. 2011;41(5):543–550.
3. Sawyer BD. Validation and insight into a novel packed-bed electrode flow battery architecture [dissertation]. Columbia: University of Missouri, 2010.
4. Suppes GJ (Inventor), University of Missouri (assignee). Convection battery configuration for connective carbon matrix electrode. US patent 20,110,206,959. August 25, 2011.
5. Gordon M, Galen S. Li-ion battery performance in convection cell configuration. *AIChE J*. In press.
6. Newman JS, Thomas-Alyea KE. Electrochemical Systems, 3rd ed. Hoboken, NJ: Wiley, 2004.
7. Newman J, Tiedemann W. Porous-electrode theory with battery applications. *AIChE J*. 1975;21(1):25–41.
8. Doyle M, Newman J, Gozdz AS, Schmutz CN, Tarascon J-M. Comparison of modeling predictions with experimental data from plastic lithium ion cells. *J Electrochem Soc*. 1996;143(6):1890–1903.
9. Fuller TF, Doyle M, Newman J. Simulation and optimization of the dual lithium ion insertion cell. *J Electrochem Soc*. 1994;141(1):1–10.
10. Doyle M, Fuller TF, Newman J. Modeling of galvanostatic charge and discharge of the lithium/polymer/insertion cell. *J Electrochem Soc*. 1993;140(6):1526–1533.
11. Kear G, Shah AA, Walsh FC. Development of the all-vanadium redox flow battery for energy storage: a review of technological, financial and policy aspects. *Int J Energy Res*. 2012;36(11):1105–1120.
12. Dunn B, Kamath H, Tarascon J-M. Electrical energy storage for the grid: a battery of choices. *Science*. 2011;334(6058):928–935.
13. Weber AZ, Mench MM, Meyers JP, Ross PN, Gostick JT, Liu Q. Redox flow batteries: a review. *J Appl Electrochem*. 2011;41(10):1137–1164.
14. Skyllas-Kazacos M, Chakrabarti MH, Hajimolana SA, Mjalli FS, Saleem M. Progress in flow battery research and development. *J Electrochem Soc*. 2011;158(8):R55–R79.
15. Srinivasan V, Newman J. Discharge model for the lithium iron-phosphate electrode. *J Electrochem Soc*. 2004;151(10):A1517–A1529.
16. Srinivasan V, Newman J. Design and optimization of a natural graphite/iron phosphate lithium-ion cell. *J Electrochem Soc*. 2004;151(10):A1530–A1538.
17. Li X, Zhang H, Mai Z, Zhang H, Vankelecom I. Ion exchange membranes for vanadium redox flow battery (VRB) applications. *Energy Environ Sci*. 2011;4:1147–1160.
18. Berezina NP, Kononenko NA, Dyomina OA, Gnusin NP. Characterization of ion-exchange membrane materials: properties vs structure. *Adv Colloid Interface Sci*. 2008;139(1–2):3–28.
19. Salerno HLS, Elabd YA. Anion exchange membranes derived from nafion precursor for the alkaline fuel cell: effect of cation type on properties. *J Appl Polym Sci*. 2013;127(1):298–307.

20. Salerno HLS, Beyer FL, Elabd YA. Anion exchange membranes derived from nafion precursor for the alkaline fuel cell. *J Polym Sci Part B: Polym Phys*. 2012;50(8):552–562.
21. Ye Y, Elabd YA. Anion exchanged polymerized ionic liquids: high free volume single ion conductors. *Polymer*. 2011;52(5):1309–1317.
22. Hilton R, Bick P, Tekeei A, Leimkuehler E, Pfeifer P, Suppes GJ. Mass balance and performance analysis of potassium hydroxide activated carbon. *Ind Eng Chem Res*. 2012;51(26):9129–9135.

Manuscript received Nov. 9, 2012, and revision received Feb. 6, 2013.